ARTICLE

Photodissociation Exploration for Near-Visible UV Absorption of Molecular Bromine

Dong-fang Zhang, Bing Zhang*

State Key Laboratory of Magnetic Resonance and Atomic and Molecular Physics, Wuhan Institute of Physics and Mathematics, Chinese Academy of Sciences, Wuhan 430071, China; Graduate School of Chinese Academy of Sciences, Beijing 100039, China

(Dated: Received on March 16, 2007; Accepted on June 19, 2007)

The photodissociation of Br_2 was investigated within the near-visible UV absorption band. Based on the potential curves for the ground and low-lying excited states, the optical cross-sections for the discrete transitions of $C^1\Pi_u$, $B^3\Pi^+_{0u}$, $A^3\Pi_{1u}\leftarrow X^1\Sigma^+_g$ and their total energy absorption spectrum are derived, and the quantum yield of (Br+Br*) channel are determined correspondingly. The one-dimensional Landau-Zener model is used to evaluate the behavior of curve crossing during photodissociation. The results indicate that the influence of nonadiabatic mechanism, which may be caused by the electronic-vibrational interplay between the B and C states, is negligibly small for the (Br+Br*) channel. From the Landau-Zener modeling of the observed product recoil parameter $\beta_{(Br+Br)}$, the best-fit value of the coupling matrix element or coupling strength between the diabatic B and C state potentials is obtained.

Key words: Photodissociation, Time-dependent wave packet, Nonadiabatic mechanism, Landau-Zener model

I. INTRODUCTION

Molecular photodissociation is a challenging area, and the results are imperative to decode the mechanism of many chemical reactions in atmospheric and biological chemistry [1-5]. The literature is wealthy with experimental and computational reports on the properties of the lowest excited states of simple molecules such as the diatomic halogen and interhalogen molecules [6-9]. In particular, the photodissociation dynamics of compounds containing bromine has attracted a lot of attention because of their strong ozone depletion potential and function in fire extinguishing reactions [10,11]. Since the atmospheric lifetimes of bromide depend substantially on the photolytic destruction rates, it is logical to study their photodynamic behavior in order to assess their environmental impact. As a benchmark system, molecular bromine is ideally suited to studies of photodissociation involving relatively large spin-orbit (SO) interaction. Upon excitation in its near-visible UV absorption continuum (320-580 nm), the bromine atom fragments produced by the dissociation process of Br_2 are basically formed in two low-lying fine structural states, i.e. the ground Br ($4p^2P_{3/2}$) (labeled as Br) state and the spin-orbit excited Br ($4p^2P_{1/2}$) (labeled as Br*) state in the ground electronic configuration via the following way: (The required energies for each channel are given with the reaction)

$$Br_2+\hbar\omega\rightarrow(Br_2)^*\rightarrow Br+Br \qquad \Delta H=190.2 \text{ kJ/mol (i)}$$

$$Br_2+\hbar\omega\rightarrow(Br_2)^*\rightarrow Br^*+Br \qquad \Delta H=234.2 \text{ kJ/mol (ii)}$$

$$Br_2+\hbar\omega\rightarrow(Br_2)^*\rightarrow Br^*+Br^* \quad \Delta H=278.2 \text{ kJ/mol (iii)}$$

here the thermodynamic threshold for bond rupture of molecular bromine is determined as $D_0(Br-Br)=$ 190.2 kJ/mol [12]. Early spectroscopic investigations [13-20] showed that the overall shape of the near-visible UV band of Br_2 is featureless and diffuse, but exhibits resolved rovibronic structure at wavelength longer than 510 nm, albeit too weak to impress an observable "shoulder" on the net absorption profile. The general composition of this band is now well identified; it can be decomposed into its three valence components, $C^1\Pi_u$, $B^3\Pi^+_{0u}$, $A^3\Pi_{1u}\leftarrow X^1\Sigma^+_g$, and absorption to the A state is much weaker, but it can nonetheless be populated for wavelength longer than 450 nm. Correspondingly, in the red wing of the visible absorption spectrum, the optical transitions have been assigned in terms of excitation from the $X^1\Sigma^+_g$ ground state to the $A^3\Pi_{1u}$ and the $B^3\Pi^+_{0u}$ upper states, which arise from the electronic configuration $(4p\sigma)^2(4p\pi)^4(4p\pi^*)^3(4p\sigma^*)^1$. Of the three transitions that are responsible for photodissociation in near-visible UV continuum of Br_2, the B←X transition is parallel to the bond axis, while the $A^3\Pi_{1u}$, $C^1\Pi_u\leftarrow X$ transition is aligned perpendicular to the bond axis.

Unlike the light systems, the dissociation behavior of heavier isovalent species Br_2 is more complicated due to the influence of large spin-orbit coupling on the photodissociation process. The initial optical excitation of various dissociation channels is significantly distinguished, and also influences the energetic properties of dissociative potentials and coupling between them, which leads to different yields of the final products. The problem of accurate determination of the Br* quantum yield Φ^* or the spatial anisotropy parameter and its de-

*Author to whom correspondence should be addressed. E-mail: bzhang@wipm.ac.cn, Tel: +86-27-87197441

pendence on the excitation energy proved to be nontrivial, and is thus an important quantity for understanding photodissociation dynamics, which in turn has a direct correlation with the properties of potential surfaces of excited states. Furthermore, an accurate quantitative analysis of photodissociation processes in Br_2 may be very helpful for larger systems having similar electronic structure. Recent works have suggested that the nonadiabatic mechanisms in the photodissociation of diatomic halogen molecules are somewhat different due to relatively large variations in the spin-orbit interactions [21-24]. For molecular chlorine, the nonadiabatic transition can take place even between the states correlating to the different dissociation limits, e.g. from $C^1\Pi_u(1_u^{(2)})$ to the higher-lying $^3\Sigma_{1u}^+(1_u^{(3)})$ due to the small spin-orbit splitting (881 cm^{-1}). In a simple description for the molecular photodissociation dynamics by an adiabatic parameter [25], adiabaticity increases as the energy spacing between diabatic potentials is increased and nuclear velocity is decreased in the transition region. Therefore, the homogenous transition mentioned above is feasible resorting to the radial derivative coupling elements. But for the heavier molecular bromine, this mechanism should be discounted because the spin-orbit splitting is larger (3685 cm^{-1}) and Br_2 will behave more adiabatically than Cl_2. The nonadiabatic transition among the lower states with the same Ω=1_u symmetry ($1_u^{(1)}$ to $1_u^{(5)}$) in Br_2 photodissociation process and the corresponding radial derivative coupling elements have been evaluated by means of semiclassical theory [26], but investigations about the possibility of nonadiabatic mechanism among states of different symmetry are spare. Thus, the current study is expected to obtain detailed information about dissociation dynamics and further examine the transition process that causes branching or anisotropy distribution of the final products.

In this work, the photodissociation of molecular bromine at near-visible UV absorption regime was investigated. The optical cross-sections of the discrete excited states are obtained from numerical methods, which are based on the *ab initio* potentials. The quantum yield of atomic bromine fragments is also determined. The possibility for dissociation paths involving nonadiabatic mechanism that are induced by the electronic-vibrational coupling is examined, and the coupling strength between two states ($B^3\Pi_{0u}^+$ and $C^1\Pi_u$) is derived resorting to the 1D Landau-Zener model.

II. NUMERICAL METHODS

The numerical methods required to deal with the photodissociation problem involve solution of the time-dependent Schrödinger equation

$$i\hbar\frac{\partial}{\partial t}\phi(R,t) = \widehat{H}\phi(R,t) \tag{1}$$

where R is the internuclear distance and $\phi(R,t)$ depicts the time-dependent wave function.

The initial wave packets are constructed by multiplying the ground state vibrational wave function ξ_ν by the appropriate transition moment functions $M_j(R)$ [21].

$$[\phi(R,t=0)] = \begin{pmatrix} C_1(R,t=0) = M_1(R)\xi_\nu \\ C_2(R,t=0) = M_2(R)\xi_\nu \\ \vdots \\ C_n(R,t=0) = M_n(R)\xi_\nu \end{pmatrix} \tag{2}$$

where $[\phi(R,t=0)]$ denotes an ensemble of the initial wave packet $\phi_j(R,t{=}0)$ (j=1, 2, $\cdots$, n) formed on the jth excited state into matrix representations, and $M_j(R)$ is the transition moment associated with the jth excited state with the ground state.

The general solution of Eq.(1) is

$$\phi(t) = \exp\left(\frac{-i\hat{H}t}{\hbar}\right)\phi(t=0) \tag{3}$$

where $\exp(-i\widehat{H}t/\hbar)$ is the time evolution operator, used to propagate wave packet $\phi(t{=}0)$ on a manifold dissociative surface. Wave packet propagation uses a split operator (time step is $\Delta\tau$) scheme

$$\phi(R,t+\Delta\tau) = \mathrm{e}^{-i\widehat{T}\Delta\tau/2\hbar}\mathrm{e}^{-i\widehat{V}\Delta\tau/\hbar}\mathrm{e}^{-i\widehat{T}\Delta\tau/2\hbar}\phi(R,t) \tag{4}$$

After each time step, the autocorrelation function $S(t)$, is calculated:

$$S(t) = \sum_j \int_{R_{\min}}^{R_{\max}} \phi_j^*(R,t=0)\phi_j(R,t)\mathrm{d}R \tag{5}$$

The total cross-section $\sigma_{\mathrm{tot}}(\nu)$ as a function of photoexcitation frequency ν is given by Fourier transformation, which can be expressed as [17]

$$\sigma_{\mathrm{tot}}(\nu) = \frac{\pi\nu}{3c\varepsilon_0\hbar}\int_{-\infty}^{\infty}\exp\left[\frac{i(E_{\nu''}+h\nu)t}{\hbar}\right]S(t)\mathrm{d}t \tag{6}$$

where ε_0 is the permittivity of vacuum, and $E_{\nu''}$ is the energy of the initial state.

The partial cross-section of dissociation for a certain channel $\sigma_j(\nu)$ is derived by collecting the information of wave packet $\phi_j(R,t)$ at an analysis line R=R_{f}, in the asymptotic region, which is a function of excitation frequency ν [27]

$$\sigma_j(\nu) = \frac{4\pi^3\nu k_j}{3c\varepsilon_0\mu}\left|S_j(R_f,E)\right|^2 \tag{7}$$

$$S_j(R_f,E) = \frac{1}{2\pi}\int_0^{\infty}\phi_j(R_f,t)\exp\left[\frac{i(E_{\nu''}+h\nu)t}{\hbar}\right]\mathrm{d}t \tag{8}$$

where μ is the reduced mass of Br_2, and k_j is the wave vector of fragments in channel j, which is deduced from

$$k_j = \frac{\sqrt{2\mu[(h\nu - V_j(R_f)]}}{\hbar} \tag{9}$$

DOI:10.1088/1674-0068/21/01/12-20

The calculations are performed using equidistant grids for the internuclear coordinate. As wave packets reach the asymptotic region, they must be attenuated by the absorbing potential to avoid boundary reflection. The coefficients of absorbing potential are

$$D_{\rm abs}(R) = 1.0 \qquad R < R_{\rm abs} \quad (10)$$

$$D_{\rm abs}(R) = \exp(-C_{\rm opt}\Delta t)\left(\frac{R - R_{\rm abs}}{R_{\rm max} - R_{\rm abs}}\right)^{1.5} \qquad R_{\rm abs} < R < R_{\rm max} \quad (11)$$

where $R_{\rm abs}$ is the starting point of damping, and $C_{\rm opt}$ is an optimum factor for damping. Values of all parameters used in the calculations are listed in Table I. The ground state and some excited states of Br_2 in this study are obtained at the CASSCF level. In the calculations, the relevant ten electrons are set as active, and the choice of active space considering the contributions from the $\sigma_{\rm Br-Br}$, $\sigma^*_{\rm Br-Br}$, $\pi(4p_x)$, $\pi(4p_y)$, and another two virtual orbitals. The relativistic *ab initio* model potential (AIMP) effective core potential (ECP) of Seijo and Barandiaran [28] are used for Br with seven valence electrons. The CASSCF (10|8) computational procedures are enforced using the MOLCAS 5.4 quantum chemistry software [29].

TABLE I The numerical parameters to perform the time-dependent wave packet computation

Variable	Description	Value
Reduced masses	μ	72853.2195 a.u.
Range of grid	$R_{\rm min}$, $R_{\rm max}$	2.592-15.397 a_0
Number of grid points		1024
Position of $R_{\rm f}$		9.80 a_0
Time step	$\Delta\tau$	0.24188 fs
Number of time steps		8192
Start of absorbing region	$R_{\rm abs}$	10.397 a_0
Damping factor	$C_{\rm opt}$	0.015 Hartree

III. RESULTS AND DISCUSSION

A. Potential energy curves of bromine molecule

There are mainly three Ω valence states of Br_2 in the near-visible UV absorption regime, which are associated with the ground $X^1\Sigma_g^+$ state by the electric-dipole transitions: one state of the 0_u^+ symmetry ($B^3\Pi_{0u}^+$) and two states of 1_u symmetry: $A^3\Pi_{1u}$, $C^1\Pi_u$. The upper state of 1_u symmetry nearby the $C^1\Pi_u$, is the third excited state of 1_u symmetry that will correlate to the Br+Br* limit: $^3\Sigma_{1u}^+(1_u^{(3)})$, arising from the electron configuration $(4p\sigma)^1(4p\pi)^4(4p\pi^*)^4(4p\sigma^*)^1$ and is usually achievable by absorbing an ultraviolet photon. Therefore, the direct absorption to this state can be discounted since it is very unlikely to be accessible, energetically, at the excitation wavelengths of interest herein. The adiabatic potential energy curves from *ab initio* calculation are shown in Fig.1. Note that the dissociation following excitation of the $B^3\Pi_{0u}^+\leftarrow X$ transition above the thermochemical threshold leads to (Br+Br) limit, while the less strongly bound $A^3\Pi_{1u}$ and the $C^1\Pi_u$ states correlate with two ground state Br atoms only. The potential energy curve for another repulsive 1_u state ($^3\Sigma_{1u}^+$), correlating to the (Br+Br*) limit, means that potential is implicated in the proposed explanation for the non-limiting β values observed for the (Br+Br*) product recoil velocity distributions [30].

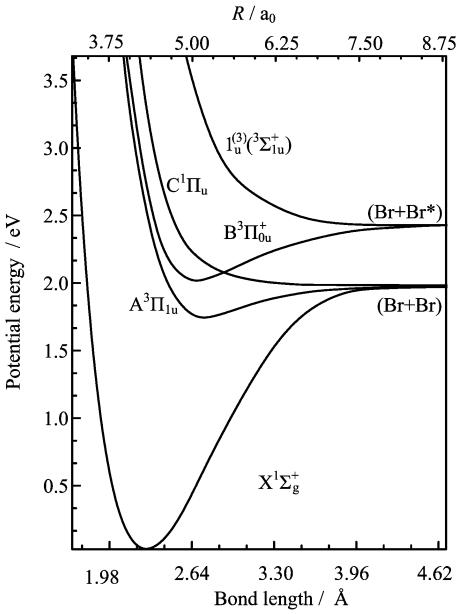

FIG. 1 Computed adiabatic potential energy curves for the $X^1\Sigma_g^+$ and Ω=1_u, 0_u^+ states correlating with two Br ($^2P_{1/2}$, $^2P_{3/2}$) atoms.

Spectroscopic constants for the X, A, and B bound states are given in Table II along with the known experimental values [12] to estimate their quality and the quality of the further calculations based on these potentials. The computed and experimental data for the bound states are found to be in reasonable agreement. One can note that the calculated equilibrium internuclear distance R_e of Br_2 (X) state are shifted to a larger interatomic separation by 0.002 Å with respect to the associated experimental data, and this effect might be a natural consequence of employing the effective core potential approach. Such systematic error is not readily sensitive to the concrete excited state and thus it can be assumed that all computed potential curves are shifted by approximately the same distance. The vibrational quantum ω_e, and constant of anharmonicity $\omega_e\chi_e$ for the computed potential is also given. The deviations from real values are within ±10 cm^{-1}.

The main deficiencies in the energy calculations appear at the intermediate and large interatomic separation and lead to an underestimation of the dissociation

DOI:10.1088/1674-0068/21/01/12-20

TABLE II Spectroscopic constants calculated in the present study for the $X^1\Sigma_g^+$, $A^3\Pi_{1u}$, and $B^3\Pi_{0u}^+$ states of Br_2 in comparison with the experimental data

State	D_e/eV		R_e/Å		ω_e/cm^{-1}		$\omega_e\chi_e$/cm^{-1}	
	Expt.	Calc.	Expt.	Calc.	Expt.	Calc.	Expt.	Calc.
$X^1\Sigma_g^+$	1.971	1.969	2.280	2.282	325.3	320.07	1.08	1.12
$A^3\Pi_{1u}$	0.2568	0.219	2.690	2.730	153	143.6	2.70	2.74
$B^3\Pi_{0u}^+$	0.4660	0.430	2.677	2.679	167.6	161.36	1.64	1.79

energies of the A, B states at equilibrium R for the corresponding state by nearly 0.0378 and 0.036 eV, respectively. This situation has no direct influence on the computed absorption spectra, however. Therefore it is expected that quantitative results can be obtained for the photodissociation processes with these *ab initio* potential energy curves.

B. The near-visible UV absorption spectra of Br_2

The near-visible UV absorption continuum of Br_2 has a maximal intensity at around 420 nm [31,32], which arises primarily due to the spin-allowed vertical excitation from $X^1\Sigma_g^+$ to the repulsive $C^1\Pi_u$ (second Ω=1_u) state. However, some states that are under the C state with nonzero electronic transition moments also can be attainable by a single photon excitation near the infrared regime (400-580 nm). With the large spin-orbit interactions, the "good" quantum number for nonrotating linear molecules such as Br_2 is the Z (along molecular axis) component of the total electronic angular momentum, namely Ω and g-u symmetry in the case of homonuclear species. The $^3\Pi_u$ state debases into four sublevels with Ω=2_u, 1_u, 0_u^-, and 0_u^+ through spin-orbit and orbit-rotation interactions, albeit the magnitude of the splitting is not significant especially in the Franck-Condon window. According to the selection rule for the spin-orbit coupling, the $A^3\Pi_{1u}$ state has a small configuration mixing with the neighboring $^1\Pi_u$ configuration. Since the $A^3\Pi_{1u}\leftarrow X$ transition borrows its intensity mostly from the $C^1\Pi_u\leftarrow X$ transition in principle, the main effect on the absorption spectra leads to a redistribution of absorption intensity between the $C^1\Pi_u$ and $A^3\Pi_{1u}$ states in favor of the latter. The $B^3\Pi_{0u}^+$ state has a small one with the higher $^1\Sigma_u^+$ configuration, and so forth. Besides, the X state has a small component of $^3\Pi_{0g}^+$ except for the chief $^1\Sigma_g^+$ component. These spin-orbit configuration mixings are the origins of the intensity borrowing of the A and B states. In this way, the $A^3\Pi_{1u}$ and $B^3\Pi_{0u}^+$ states will borrow oscillator strength from allowed transitions through one or more second-order pathways. Thus, the states that are below the C state and can be excited from the X state are the B (transition via a parallel type, $|\Delta\Omega|$=0) and A (transition via a perpendicular type, $|\Delta\Omega|$=1) states.

The absorption cross sections or coefficients are numerically calculated by employing the time-dependent wave packet dynamical method, which is based on the relevant *ab initio* potential curves. The computed absorption spectra to the A, B, and C state are illustrated in Fig.2. The peak wavelength of the absorption band to the C state is about 417.6 nm, in accord with the experimental data, which is 420 nm by Oldman *et al.* [17]. The theoretical peak intensity of the visible absorption band is weaker than the experimental one (Passchier *et al.* [33]) of about 2.618 cm^2/molec. And as wavelength is shorter than 450 nm, the absorption is dominated absolutely by transitions to the repulsive $C^1\Pi_u(1_u)$ state. The peak wavelength of B state appearing at 485 nm, is consistent with the observation of about 480 nm by Haugen *et al.* [14], while the A state peaks at around 530 nm, in accord with the prediction by Coxon [34], although it is larger than the theoretical assignment made by Oldman that the position lies at 500 nm. It is also clear that the $A^3\Pi_{1u}\leftarrow X$ is not significant as $\lambda\leq$500 nm and at 510 nm, the contribution of the A state is only about 21% of the total absorption. The peak intensity of the absorption band to the A state is about 7.72% of that to the C state, while that to the B state is about 38.3% of that to the C state. These two weaker absorption peaks, nevertheless, emerge far from the peak position of the C state, and their relative intensities become more prominent in the longer wavelength range. Therefore, the A and B states are anticipated to make a significant devotion there, despite their weaker intensities. The partial absorption spectra of A, B states

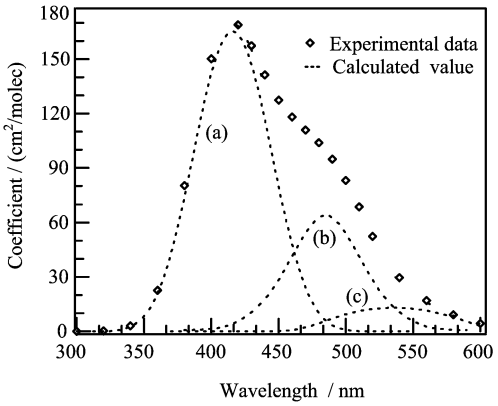

FIG. 2 Extinction coefficient as a function of excitation wavelength. (a) $C^1\Pi_u\leftarrow X$, (b) $B^3\Pi_u\leftarrow X$, (c) $A^3\Pi_{1u}\leftarrow X$. Experimental data was from Ref.[33].

DOI:10.1088/1674-0068/21/01/12-20

indicate that the A-X and, particularly, B-X transition, which still can dedicate to the continuous absorption for wavelengths less than 510 nm.

To show accuracy of the calculations, the total absorption coefficient are compared with the available experimental data of Passchier *et al.*, the latter is the electronic absorption spectrum of Br_2 recorded over the wavelength range of 320-580 nm at temperature of 298 K. Regardless of the fact that the general shape and intensity of computation closely resemble that actually observed with the path length employed, there are mild deviations in the magnitude of total profile near the intermediate region of the this near-visible UV spectrum band. For instance, the extinction intensity is calculated to be 76.15 cm^2/molec at 480 nm, the corresponding measured value is 82.66 cm^2/molec. It also can note the defects only become visible from the beginning of about 440 nm, particularly in the energy range of 470-510 nm, in which a considerable part of the optical extinction is rightly dominated by the occurrence of $B^3\Pi^+_{0u}\leftarrow X^1\Sigma^+_g$ transition. The curvature of intensity profile changes in some sort around 475 nm, which may be attributed to the participation of A, B←X electronic transition.

An alternative test of the accuracy of the present calculations is provided by the available experimental data for the final product distribution in the Br_2 photofragmentation, as will be discussed in the next section.

C. Quantum yield for the [Br+Br*] channel

With the intention of further characterizing the nature and roles of the excited states or various participating channels involved in the photodissociation dynamics of Br_2, the quantum yield for product channel (ii) after optical absorption from the X state has been estimated in the present work, which is expressed in the adiabatic approximation as

$$\begin{aligned}\phi_\lambda(\mathrm{Br}+\mathrm{Br}^*) &= \frac{\sigma[\mathrm{Br}+\mathrm{Br}^*]}{\sigma[\mathrm{Br}+\mathrm{Br}^*]+\sigma[\mathrm{Br}+\mathrm{Br}]} \\ &= \frac{\sigma_{\text{B-X}}(\nu)}{\sigma_{\text{tot}}(\nu)} \qquad (12)\end{aligned}$$

where σ[Br+Br*] and σ[Br+Br] are, respectively, the optical cross sections of (Br+Br*) and (Br+Br) channel following photodissociation. In this case, it means the relative fraction of total absorption $\sigma_{\text{tot}}(\nu)$ leads to population of the $B^3\Pi^+_{0u}$ state, i.e. $\sigma_{\text{B-X}}(\nu)$ at each wavelength λ. The experimental data [14,15,35] ϕ_λ for (Br+Br*) channel are depicted in Fig.3, which are compared with the dynamical prediction through wave packet simulation. Based on the energy ordering of states in the Franck-Condon region: at the shortest wavelengths (λ<440 nm) ϕ is small, reflecting the relative strength of the $C^1\Pi_u(1_u)\leftarrow X^1\Sigma^+_g(0^+_g)$ transition, which causes the preferential formation of (Br+Br) over (Br+Br*); however, within the intermediate wavelength

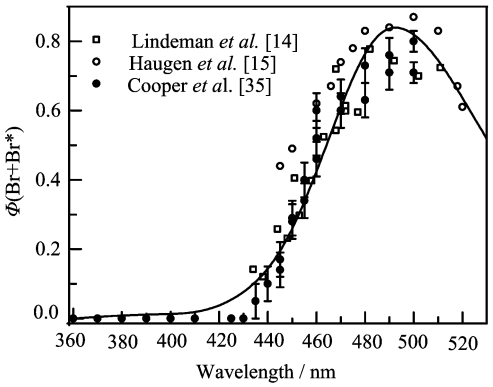

FIG. 3 Br+Br* photofragment quantum yield ϕ(Br+Br*), plotted as a function of excitation wavelength. Solid line was from wave packet calculations.

range (λ=460-510 nm), (Br+Br*) photofragments are formed in excess of (Br+Br), signifying a dominance in this region of the $B^3\Pi^+_{0u}(0^+_u)\leftarrow X^1\Sigma^+_g(0^+_g)$ transition. With excitation at longer wavelengths (λ>520 nm), the resultant quantum yield ϕ is also predicted to be comparatively lower, indicating the prevalence of the $A^3\Pi_{1u}(1_u)\leftarrow X^1\Sigma^+_g(0^+_g)$ transition. The threshold wavelength for producing the combinations of $Br(^2P_{3/2})$ and $Br^*(^2P_{1/2})$ atoms via photodissociation is λ<510.6 nm and energetic considerations dictate that the (Br+Br*) active channel is only possible from photolysis of the Br_2 molecule in its ν''=0 level at wavelengths around 520 nm. Thus the present data on the photofragment quantum yield are very sparse for photolysis wavelength region of λ>510 nm except for Haugen *et al.*, which extend their measurements till λ=530 nm. For this reason we make an effort to define the wavelength dependence of the deduced quantum yield into the (Br+Br*) product channel within the truncation of $\lambda\leq$530 nm. It also should be noted that the experimental data from Cooper and Lindeman *et al.* are in reasonable agreement with the present work within the error allowance, except at the intermediate wavelengths (λ=450-500 nm), where the calculated function suggests smaller values of ϕ relative to the data sets of Haugen *et al.*.

In the adiabatic representation of the PESs for the Br_2 system, the electronic Hamiltonian (now including spin-orbit coupling) is diagonalized to create Born-Oppenheimer PESs and the correlations of PESs with product channel shown in Fig.1 are strict. Once the nature of the PESs that is initially populated is established, the asymptotic product channel with which the PES correlates is also determined. Therefore, the quantum yield ϕ_λ(Br+Br*) following photolysis of Br_2 at wavelengths in this regime of 320-580 nm should be consistent with the expected behavior of the energy dependence of the partial cross-sections for transitions A, B, C←X strictly. However, a minor discrepancy still exists between the calculation and measurement. Pro-

DOI:10.1088/1674-0068/21/01/12-20

vided that the systematical and random error in experiment can be safely disregarded, this will mean that the influence of nonadiabatic mechanism on the photodissociation process may be underestimated more or less. In most cases, as the system evolves from the vicinity of the equilibrium (short range) internuclear distance to regions of large separation, the Born-Oppenheimer approximation breaks down. For that reason, at the asymptotic limit, the electronic quantum states of the photofragments will reflect both the initial absorption and the degree of mixing between different electronic energy states at extended bond lengths. Thus, one possible reason for the deviation from the experimental ϕ_λ(Br+Br*) values may be the ignorance of the necessary perpendicular contribution arising from the constructive interference at the larger interatomic distance between the translational wavefunction associated with the initially populated state of 1_u symmetry such as $A^3\Pi_{1u}(1_u)$ state, or possibly, the $C^1\Pi_u(1_u)$ state, from which the subsequent nonadiabatic coupling to other Ω=1 states nearby the asymptotic region, and where the exchange interaction is not important. In particular, coupling to the $^3\Sigma^+_{1u}(1^{(3)}_u)$ state, which correlates to the (Br+Br*) dissociation limit and forms the (Br+Br*) photofragments adiabatically. If coupling only takes place between the electronic surfaces of A and C states, the quantum yield ϕ will not be affected due to these two states converge explicitly to the same end product (Br+Br) asymptote. In conclusion, it should be emphasized that it is quite difficult to make unambiguous conclusions about the reason for this discrepancy, nevertheless, since it is not large and too many parameters and details can influence the final result.

D. Adiabatic versus diabatic description on photodissociation

For the formation of (Br+Br*) cofragments, the $B^3\Pi^+_{0u}(0^+_u)\leftarrow X^1\Sigma^+_g(0^+_g)$ transition is involved, which consists of a major contribution to the overall absorption in the wavelength range of λ=450-500 nm. Therefore, initially populated by direct excitation and fragmentation via the B state (i.e., $\Delta\Omega$=0, parallel type) should lead to Br*+Br products with a product flux recoil velocity distribution characterized by an ideal value of β=+2.0. However, the facts indicate a reverse situation. In practice, the best-fit $\beta \approx 1.5$ at the shorter wavelengths but falls to $\beta \approx 0.6$ at 500 nm.

Thus, elucidating the obtained wavelength dependent of β throughout the active range of the (Br+Br*) product channel is not trivial. To achieve this goal, some influential factors should be taken into account. For instance, consider dissociation events that happen on a time scale that is slower than the rotational period of parent molecule such as spontaneous predissociation; logically this has the outcome of dropping the anisotropic by nearly half, but this mechanism can be easily ruled out since the reduction of β is usually negligible in terms of a rigid impulsive model [36], thus the effect of rotational motion on angular distribution for direct dissociation can be ignored. Furthermore, the direction dissociation is an ultrafast process. Molecules decay in several femtoseconds after absorbing a photon (i.e., $\tau_{dis}\approx10^{-15}$ s) [37], but the rotational period is of nanosecond magnitude for the majority of small molecules, so actually $\tau_{dis}\ll\tau_{rot}$ should be correct. If the non-axial recoil does hold, this situation is salient only for those high rotationally excited molecules, while using a supersonic beam the temperature is low enough to suppress the quasi-rotational frequencies, as done previously [35]. The last possibility can be ascribed to in-phase transitions to multiple electronic states of different symmetry that correlate to the same separated-atom asymptote. Nevertheless, it is hard to explain since the $C^1\Pi_u(1_u)$ state has invalid symmetry to make angular distribution of fragments described by a positive β value. Therefore, the recoil parameter in observation may come from the quantum mechanical interference between two or more dissociating states with different symmetries. If this mechanism is sound, the observed $\beta_{(Br^*+Br)}$ values can be readily explained by assuming that most of these products are originated from direct dissociation of molecular bromine prepared in the $B^3\Pi^+_{0u}(0^+_u)$ potential, and a fraction of the (Br+Br*) products arise via an alternative or perpendicular route. This is possible because each of the B state level with $\nu''>0$ level above the lowest energy (Br+Br) dissociation limit and are subject to predissociation by coupling to a repulsive state of 1_u symmetry. Thus, the nonadiabatic mechanism, which may be induced by electronic-vibrational coupling, can be viewed as a possibility with transfer of flux between two states of $B^3\Pi^+_{0u}$ and $C^1\Pi_u$ potential is assumed.

The present discussion will be couched entirely in terms of diabatic potentials and a coupling parameter $V_{B/C}$, which represents the interaction strength between $B^3\Pi0^+_{0u}$ and $C^1\Pi_u$ states. Opposed to symmetry-required intersections, which occur between two degenerate electronic excited states that belong to the same irreducible representation, the accidental intersections correspond to intersections that occur in a coordinate subspace where the symmetry does not play a role. According to the noncrossing rule [38], intersections between states of the same symmetry are permitted in a space of dimension K-2, namely the seam space, where K is the number of internal degrees of freedom. Thus, in diatomic molecule, only states of different symmetry can cross and even cross freely, which remains valid for B and C states in Br_2. The curve crossing probability is rationalized by the one-dimensional Landau-Zener based model [39,40]. Using this model, it is possible and instructive to determine the fraction of molecule initially excited to the C state potential which dissociate adiabatically to (Br+Br) and those which follow the diabatic route, i.e., transferring to the diabatic B

DOI:10.1088/1674-0068/21/01/12-20

potential and yield (Br+Br*). Following the Landau-Zener description, the probability of curve crossing is given by

$$\begin{aligned} P &= 1-\exp\left(\frac{-2\pi V_{12}^2}{\hbar|\Delta F|\upsilon_{\rm cc}}\right)=1-\exp\left(\frac{-\zeta}{\upsilon_{\rm cc}}\right) \\ \Delta F &= \left|\frac{\rm d}{{\rm d}r}[V_{\rm c}(r)-V_{\rm B}(r)]\right|_{r=r_{\rm c}} \end{aligned} \tag{13}$$

where V_{12} is the coupling term between the diabatic potential, ΔF is the difference in potential slopes at the crossing point $r_{\rm c}$, and $\upsilon_{\rm cc}$ is the velocity through the crossing point. The Landau-Zener parameter ζ includes V_{12} and ΔF terms, is characterized only by the potential energy surface of the molecule, and is independent of excitation energy, so it is constant for a given molecule. For the excitation of specific photon energy, crossing velocity $\upsilon_{\rm cc}$ is calculated from

$$\upsilon_{\rm cc}=\sqrt{2E_0/\mu}, \qquad E_0=E_{h\nu}-E_x \tag{14}$$

where μ is the reduced mass of Br_2 molecule, $E_{h\nu}$ the photon energy, and E_0 and E_x, the translational and potential energy of fragments at the crossing point respectively. This suggests that the less energy released in translation during the photodissociation processes, the slower the passage through the crossing region and the greater the chance of curve crossing between the two excited states. Given the B and C state potential shown in Fig.1, E_x=16764.6 cm^{-1}, $r_{\rm c}$=2.90 Å, $V_{\rm B}'(r_c)$=2566.3 cm^{-1}Å^{-1}, $V_{\rm C}'(r_{\rm c})$=−3226.2 cm^{-1}Å^{-1}. Here primes (′) denote differentiation with respect to internuclear distance variable r. Then ΔF=5792.5 cm^{-1}Å^{-1}. The crossing probability $P_{\rm diab}$ in experiment from the diabatic C state to the B state, should be derived by considering the angular distributions of the fragmentation product channel (Br+Br*). The angular distribution $P(\theta)$ can be fitted into the standard formula [41]

$$\begin{aligned} P(\theta) &\propto 1+\beta_{\rm eff}P_2\cos\theta \\ &= 1+\beta_{\rm eff}\left(\frac{3}{2}\cos^2\theta-\frac{1}{2}\right) \end{aligned} \tag{15}$$

where $P_2(\cos\theta)$ is the second-order Legendre polynomial, and θ indicates the angle between ϵ vector of the photolysis laser radiation and the direction of photofragment recoil. In order to calculate an effective anisotropy parameter ($\beta_{\rm eff}$) for the (Br+Br*) product flux at any given wavelength λ, the P-distribution of the fragments is represented as

$$\begin{aligned} P(\theta) &\propto P_{\parallel}(\theta)+AP_{\perp}(\theta) \\ P_{\parallel}(\theta) &= (2/3\pi)\cdot(1+2P_2\cos\theta)=2\cos^2\theta/\pi \\ P_{\perp}(\theta) &= (4/3\pi)\cdot(1-P_2\cos\theta)=2\sin^2\theta/\pi \end{aligned} \tag{16}$$

where $P_{\parallel}(\theta)$ and $P_{\perp}(\theta)$ are normalized angular distribution for the two limiting cases β=+2 (parallel transition) and β=−1 (perpendicular transition), respectively, and A is the coefficient of the perpendicular component. Then the effective beta parameter $\beta_{\rm eff}$ can be determined by fitting I^* angular distributions with functional form of $P(\theta)$, and it can be found that

$$A=\frac{2-\beta_{\rm eff}}{2(1+\beta_{\rm eff})} \tag{17}$$

The probability of crossing $P_{\rm diab}$, for Br to be converted into a Br* is explicitly given by the relationship that $P_{\rm diab}$=$f(\mathrm{C}^1\Pi_{\rm u}\rightarrow\mathrm{B}^3\Pi_{0\rm u}^+)/f(\mathrm{C}^1\Pi_{\rm u})$, and $f(\mathrm{C}^1\Pi_{\rm u})$ is the fraction of the total absorption that initially populates the $\mathrm{C}^1\Pi_{\rm u}$ surface, while $f(\mathrm{C}^1\Pi_{\rm u}\rightarrow\mathrm{B}^3\Pi_{0\rm u}^+)$ is the relative fraction of perpendicular component for (Br+Br*) channel. Since A denotes the fraction of Br* fragments via the curve crossing from $\mathrm{C}^1\Pi_{\rm u}$ to the $\mathrm{B}^3\Pi_{0\rm u}^+$ surface to overall Br* fragments, it can be estimated from the effective anisotropy parameter or angular distribution of final product. In conclusion, the above formula therefore can be transformed into

$$P_{\rm diab}=\frac{A\sigma_{\rm tot}(\nu)\Phi({\rm Br}+{\rm Br}^*)}{\sigma_{\rm C\text{-}X}(\nu)} \tag{18}$$

where $\sigma_{\rm tot}(\nu)$ is the total energy cross-section in photolysis, $\sigma_{\rm C\text{-}X}(\nu)$ denotes the partial cross-section of continuum transitions for $\mathrm{C}^1\Pi_{\rm u}\leftarrow$X, and Φ (Br+Br*) is the experimental quantum yield of (Br+Br*) fragmentation channel. According to the theory, if nonadiabatic mechanism caused by the coupling matrix element in the diabatics (B and C states), the curve-crossing behavior should follow the Landau-Zener (LZ)-type relationship. Since ζ is a constant, and the velocity $\nu_{\rm cc}$ at the crossing point of the two potentials depends on a specific wavelength λ, therefore the magnitude and frequency dependence of $P_{\rm diab}$ relative to the photolysis energy will be governed by the parameter ζ of coupling force characteristic, which can be examined by performing a Landau-Zener type fitting.

As is evident from Fig.4, the Landau-Zener prediction agrees approximately at high photon energies and deviates strongly from that obtained refer to literature [15,35] as the photolysis energy decreases. In addition, the failure of this model from a global perspective may suggest that the possibility of a nonadiabatic mechanism induced by the electronic-vibrational coupling, which connects two adiabatic states (B and C) with different symmetry (Ω=0 and Ω=1 respectively), is negligibly small. From this, the contribution of the electronic-vibrational interaction for the production of (Br+Br*) can be neglected rationally.

To examine if the nonadiabatic mechanism holds for the (Br+Br) fragmentation channel, the Landau-Zener model is applied for the $Br_2\rightarrow$Br+Br dissociation path by taking into account the strength of the B/C interstate coupling ($V_{\rm B/C}$) in the vicinity of their crossing point. Given the relative magnitudes of the Br*/Br spin-orbit splitting ($E_{\rm so}$ is 3685.24 cm^{-1}), the coupling term linking the diabatic B and C states can be viewed as a small perturbation compared with the asymptotic

DOI:10.1088/1674-0068/21/01/12-20

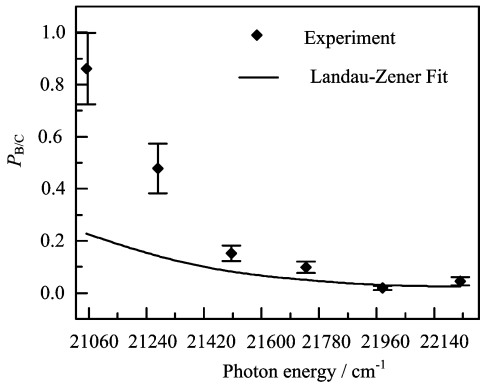

FIG. 4 Plot showing the derived probability of the B/C curve crossing.

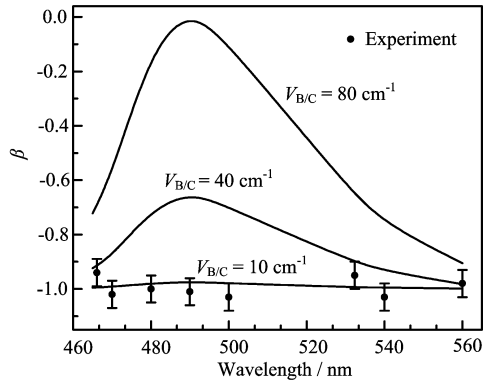

FIG. 5 Experimentally determined anisotropy parameter β for (Br+Br) channel and with those derived from theoretical analysis by assuming a variety of B/C coupling constants.

separation of the B and C state potentials, and thus $V_{B/C}$ is treated as constant. Here, the amplitude of this coupling term is set as adjustable to produce an acceptable fit to the experimental data, and the frequency dependence of curve crossing probability P_{cc} is extracted by including the magnitude of $V_{B/C}$ into the assessment. Under this description, within the confines of the potentials shown in Fig.1, wave packets launched on the B state potential, however, will bifurcate in the region where this potential crosses with that of the diabatic C state, to an extent that will depend on the strength of the B/C state coupling and only that portion of the wave packet launched on the diabatic B state potential that remains on this potential will reach the analysis line at the Br+Br* asymptote. Conversely, the diabatic potentials of the A and C states both converge to the Br+Br asymptote. The two latter potentials are achieved via a perpendicular transition from the $X^1\Sigma_g^+$ state, and flux evolving on these two potentials will display recoil distribution of a pure perpendicular character. In terms of the foregoing, $\beta_{(Br+Br)}(\nu)$ will thus be given by

$$\beta_{(Br+Br)}(\nu) = \frac{2\sigma_{B\text{-}X}(\nu)P_{cc} - \sigma_{A\text{-}X}(\nu) - \sigma_{C\text{-}X}(\nu)}{\sigma_{A\text{-}X}(\nu) + \sigma_{C\text{-}X}(\nu) + \sigma_{B\text{-}X}(\nu)P_{cc}} \quad (19)$$

where $\sigma_{j-X}(\nu)$ (j=A, B, C) denotes the partial cross-section for an optical transition associated with the X state.

Figure 5 shows the experimental measured β parameter [35] for the Br+Br products and theoretical β parameter with its frequency dependence, which assuming the coupling strength $V_{B/C}$ to be in the range of 10-80 cm^{-1}, and the analysis made following photolysis at wavelengths λ=465-560 nm. It could be found that a best-fit coupling matrix element is derived as $V_{B/C}$=10 cm^{-1}, which successfully reproduces most of the observed phenomena within the error limit. By comparison, the experimental one only could be approximately replicated at λ=465, 560 nm by assuming the strength of the B/C coupling equal to 40 cm^{-1}. In addition, the deduced β function appears to divert from the genuine form of the measured recoil anisotropies by assuming $V_{B/C}$=80 cm^{-1}, which serves to affirm that this type of coupling term is completely unlike to be the actual interaction between the B and C state potentials. In light of the optimal value of $V_{B/C}$ that in modeling the energy dependent β anisotropy coefficient, the role of nonadiabatic mechanism in the dissociation processes of Br_2 photolysis will be clear. The transfer of flux from the $B^3\Pi_{0u}^+$ state into the Br+Br limit is not worth considering due to the strength of the B state coupling to the C state is not large ($V_{B/C}\approx$10 cm^{-1}). So the obtained (Br+Br) atoms should come from channel only with perpendicular polarization, in such case is provided by photoexcitation to the A or C state. A similar example is HI system, the localized matrix element of the spin-rotational operator gives the same magnitude order, and it is found that the inclusion of this coupling does not have striking effect on the reaction path [42]. If we cogitate that the strength of electronic-vibrational operator usually greater than that from spin-rotational, the effective matrix element of electronic-vibrational operator should be 30 cm^{-1} approximately.

Associated with the present discussion on the action that curve crossing plays in the (Br+Br) fragmentation channel, the situation for the formation of (Br+Br*) is more transparent. Since the corresponding nonadiabatic interaction, which has an electronic-vibrational nature, is slim. Therefore, such nonadiabatic mechanism should be of negligible importance perhaps within the 100 cm^{-1} energy interval near the crossing. Hence the perpendicular contribution to dissociation channel (ii) observed at longer excitation wavelengths can just be ascribed to configuration mixing of exit channel between A and $^3\Sigma_{1u}^+$ state rather than the nonadiabatic transfer from the $C^1\Pi_u(1_u)$ state. Besides, the crossing of the B and C states lies very low: E_x=16764.6 cm^{-1} (λ=596.49 nm) in this near-visible UV absorption band, the $B^3\Pi_{0u}^+ \leftarrow X^1\Sigma_g^+$ transition is much stronger than $C^1\Pi_u \leftarrow X^1\Sigma_g^+$ at such excitation energies. So that curve hopping would more favorable for the yield of (Br+Br)

DOI:10.1088/1674-0068/21/01/12-20

than the formation of (Br+Br*) coming from the parallel photoexcitation. The fact that no significant parallel component of the (Br+Br) product channel reflected in experiment strongly supports the above conclusion that the contribution of the nonadiabatic mechanism, which may be rendered by electronic-vibrational coupling, is negligible for the near-visible band photofragmentation of Br_2.

IV. CONCLUSION

The photodissociation of Br_2 was studied between 320-580 nm in its near-visible UV continuum band. From the wave packet calculations on *ab initio* potential energy curves, the partial absorption spectra for transitions from $X^1\Sigma_g^+$ (ν''=0) to the $A^3\Pi_{1u}$, $B^3\Pi_{0u}^+$, $C^1\Pi_u$ states and the total absorption spectrum of this band are determined. The quantum yield for the (Br+Br*) channel is predicted theoretically and is found to be in reasonable agreement with the experimental phenomena. The crossing behavior is analyzed by employing the Landau-Zener model. The results suggest that the nonadiabatic mechanism invoked by electronic-vibrational coupling can be ignored for the (Br+Br*) exit channel. According to this model, the strength for B state coupled to the C state is set as adjustable in the calculation of recoil parameter $\beta_{(Br+Br)}$ and a coupling matrix element $V_{B/C}$=10 cm^{-1} is found to successfully reproduce the frequency dependence of the recoil anisotropy of (Br+Br) fragmentation channel.

V. ACKNOWLEDGMENT

This work was supported by the National Natural Science Foundation of China (No.10534010 and No.20673140).

[1] S. J. Riley and K. R. Wilson, Faraday Discuss **53**, 132 (1972).
[2] M. Dzvonik, S. Yang, and R. Bersohn, J. Chem. Phys. **61**, 4408 (1974).
[3] M. H. Alexander and S. L. Davis, J. Chem. Phys. **78**, 6754 (1983).
[4] P. Houston, Annu. Rev. Phys. Chem. **40**, 375 (1989).
[5] J. P. Doering, J. Chem. Phys. **67**, 4065 (1977).
[6] H. Kato and M. Baba, Chem. Rev. **95**, 2311 (1995).
[7] M. C. Heaven, Chem. Soc. Rev. **15**, 405 (1986).
[8] H. Okabe, *Photochemistry of Small Molecules*, New York: Wiley, 217 (1978).
[9] S. R. Leone, *Dynamics of the Excited State*, K. P. Lawley, Ed., New York: Wiley, 255 (1982).
[10] Y. L. Yung, J. P. Pinto, R. J. Watson, and S. P. Sander, J. Atmos. Sci. **37**, 339 (1980).
[11] R. P. Wayne, *The Chemistry of Atmospheres*, 2nd. New York: Oxford University Press, (1991).
[12] K. P. Huber and G. Herzberg, *Molecular Spectra and Molecular Structure, IV. Constants of Diatomic Molecules*, 2nd Ed, New York: Van Nostrand Reinhold, 325 (1979).
[13] C. P. Hemenway, T. G. Lindeman, and J. R. Wiesenfeld, J. Chem. Phys. **70**, 3560 (1979).
[14] H. K. Haugen, E. Weitz, and S. R. Leone, J. Chem. Phys. **83**, 3402 (1985).
[15] T. G. Lindeman and J. R. Wiesenfeld, J. Chem. Phys. **70**, 2882 (1979).
[16] R. J. Le Roy, R. G. Macdonald, and G. Burns, J. Chem. Phys. **65**, 1485 (1976).
[17] R. J. Oldman, R. K. Sander, and K. R. Wilson, J. Chem. Phys. **63**, 4252 (1975).
[18] M. A. A. Clyne and M. C. Heaven, J. Chem. Phys. **76**, 5341 (1982).
[19] J. E. Smedley, H. K. Haugen, and S. R. Leone, J. Chem. Phys. **86**, 6801 (1987).
[20] J. E. Smedley, H. K. Haugen, and S. R. Leone, J. Chem. Phys. **87**, 2700 (1987).
[21] A. S. Bracker, E. R.Wouters, A. G. Suits, and O. S. Vasyutinskii, J. Chem. Phys. **110**, 6749 (1999).
[22] A. J. Alexander, Z. H. Kim, S. A. Kandel, R. N. Zare, T. P. Rakitzis, Y. Asano, and S. Yabushita, J. Chem. Phys. **113**, 9022 (2000).
[23] T. P. Rakitzis and T. N. Kitsopoulos, J. Chem. Phys. **116**, 9228 (2002).
[24] M. J. Bass, M. Brouard, A. P. Clark, C. Vallance, and B. Martinez-Haya, Phys. Chem. Chem. Phys. **5**, 856 (2003).
[25] Y. L. Huang and R. J. Gordon, J. Chem. Phys. **94**, 2640 (1991).
[26] Y. Asano and S. Yabushita, Chem. Phys. Lett. **372**, 348 (2003).
[27] P. M. Regan, D. Ascenzi, A. Brown, G. G. Balintkurti, and A. J. Orr-Ewing, J. Chem. Phys. **112**, 10259 (2000).
[28] Z. Barandiaran and L. Sijo, Can. J. Chem. **70**, 409 (1992).
[29] K. Andersson, M. P. Fulscher, R. Lindh, P. A. Malmqvist, J. Olsen, B. O. Roos, A. J. Sadlej, and P. O Widmark, *MOLCAS Version 5.4*, Sweden: University of Lund. (2000).
[30] Y J. Jee, M. S. Park, Y. S. Kim, Y. J. Jung, and K. H. Jung, Chem. Phys. Lett. **287**, 701 (1998).
[31] S. Hubinger and J. B. Nee, J. Photochem. Photobiol, A. **86**, 1 (1995).
[32] J. Tellinghuisen, J. Chem. Phys. **115**, 10417 (2001).
[33] A. A. Passchier, J. D. Christian, and N. W. Gregory, J. Phys. Chem. **71**, 937 (1967).
[34] J. A. Coxon, J. Mol. Spectrosc. **37**, 39 (1971).
[35] M. J. Cooper, E. wrede, A. J. Orr-Ewing, and M. N. R. Ashfold, J. Chem. Soc. Faraday Trans. **94**, 2901 (1998).
[36] A. F. Tuck, J. Chem. Soc. Faraday Trans. **73**, 689 (1977).
[37] M. Dzvonik, S. Yang, and R. Bersohn, J. Chem. Phys. **61**, 4408 (1974).
[38] J. V. Neumann and E. Wigner, Phys. Z. **30**, 647 (1929).
[39] E. E. Nikitin, *Theoty of Elementary Atomic and Molecular Processes in Gases*, New York: Oxford University Press, 107 (1974).
[40] R. D. Levine and R. B. Bernstein, *Molecular Reaction Dynamics and Chemical Reactivity*, New York: Oxford University Press, 377 (1987).
[41] R. N. Zare, Mol. Photochem. **4**, 1 (1972).
[42] N. Balakrishnan, A. B. Alekseyev, and R. J. buenker, Chem. Phys. Lett. **341**, 594 (2001).

DOI:10.1088/1674-0068/21/01/12-20